Application of the Filippov method for the stability analysis of a photovoltaic system

Cristina Morel, Dorin Petreus, Adina Rusu

Application of the Filippov Method for the Stability Analysis of a Photovoltaic System

Cristina MOREL[1], Dorin PETREUS[2], and Adina RUSU[2]
[1]*ESEO Group, Graduate School of Engineering, Angers, 49009, France*
[2]*Technical University of Cluj-Napoca, Applied Electronics Depart., Cluj-Napoca, 400027, Romania*
cristina.morel@eseo.fr

***Abstract*—This paper describes bifurcation phenomena of a photovoltaic system. The studied photovoltaic (PV) system includes a solar panel, a boost converter, a maximum power point tracking (MPPT) controller and a storage device. Computer simulations are performed to capture the effects of variation of some chosen parameters on the qualitative behavior of the system. The impact of the maximum power point (MPP) current and voltage variations due to luminosity changes is determinate, as well as the load variation. The stability of the system is analyzed using the state transition matrix over one switching cycle (the monodromy matrix) including the state transition matrices during each switching (the saltation matrices). This investigation is important to predict nonlinear phenomena and for the components dimensioning for a proper functioning.**

***Index Terms*—photovoltaic systems, dc-dc power converters, nonlinear dynamical systems, bifurcation, chaos, monodromy matrix, saltation matrix.**

I. INTRODUCTION

Energy harvesting from alternative energy resources is looking to become a preferred solution to the polluting and expensive conventional resources like oil and gas. Solar energy is known to produce no pollution during operation; therefore all the concerns focus on processes regarding the manufacturing and installation, the amount of land occupied and wildlife protection.

In general, the main components of a standalone solar system are the PV module - that converts solar energy into electrical energy, a dc-dc converter - that converts the PV voltage level into a higher or lower level, depending on the load requirements, a digital controller - implementing a MPPT algorithm to ensure the system operation at MPP and a storage device - where the energy is accumulated for further use (Fig. 1) [1] – [4].

Systems using MPPT controllers [5] have better performance than directly connected systems. Solar tracker systems can generate up to 35 per cent more power than fixed PV systems, and ensure maximum productivity even during periods of weak or low sunlight [6], [7]. The MPPT algorithms measure the solar module output current and voltage, and determine an adjustment of a control parameter, usually the duty ratio of the dc-dc converter [5] – [8].

A large number of methods have been introduced in the recent years to improve the precision and time response of MPPT control.

Algorithms like perturb and observe or incremental conductance are easy to implement but might present oscillations around the MPP, while fuzzy control, genetic algorithms or neural network prediction are more precise but also more complex, requiring more processing time and computational power. The same method may have different versions of implementation in order to obtain the desired performance, depending on the hardware architecture.

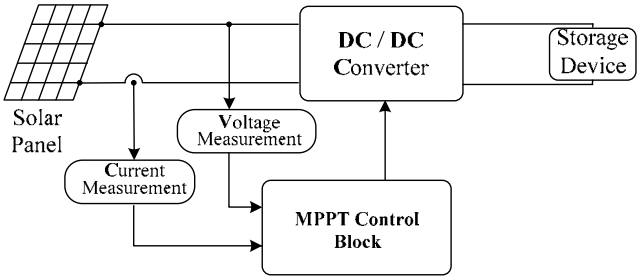

Figure 1. Block diagram of a solar system.

After the study of the harmonics of chaotic systems [9] and the generation of independent attractors [10]-[11], it is interesting now to see the potentially chaotic behaviour of photovoltaic systems [3], [4].

In this paper, the dynamic behavior of a PV system is analyzed; its stability and the conditions where it exhibits chaos or quasi-periodic nonlinear characteristics are discussed.

II. THE PRINCIPE OF MPPT CONTROL

The first step in the development of a complete solar photovoltaic conversion system (Fig.1) is the PV module electrical model. A circuit based model for a solar cell was implemented in Matlab®, thus allowing the simulation of the dependence on the irradiance and temperature. The single-diode model presented in Fig. 2 is described by Eq. (1).

$$I_{PV} = I_{ph} - I_O\left[exp\left(\frac{V_{PV} - I_{PV}\cdot R_S}{nkT}\right) - 1\right] - \frac{V_{PV} + I_{PV}R_S}{R_{sh}} \quad (1)$$

I_{ph} is the solar cell photocurrent, directly proportional to solar irradiance S [W/m^2].

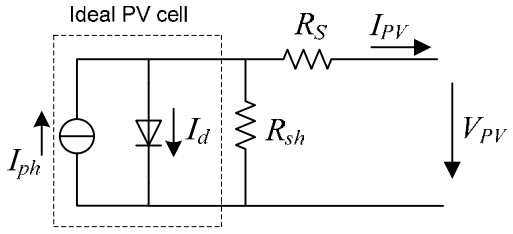

Figure 2. Single-diode equivalent circuit of a photovoltaic cell.

The resistance R_S depends on the resistance inside each cell between its layers and on the connection between cells. The shunt resistance R_{sh} corresponds to the leakage current to the ground and is commonly neglected to simplify the model, since it generally has a high value. R_S influences the device functioning in the voltage source operation region, while R_{sh}'s influence is in the current source operation region. The device is modeled [12] using a single diode with the quality factor set to achieve the best curve match.

A typical I-V characteristic of a solar cell for different levels of irradiation S and a fixed cell temperature T=25° C, is shown in Fig. 3 and Fig. 4. The output of the current source is directly proportional to the light falling on the cell.

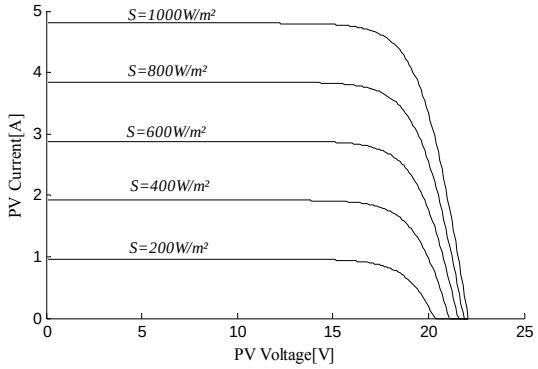

Figure 3. PV I-V characteristic for several irradiation levels.

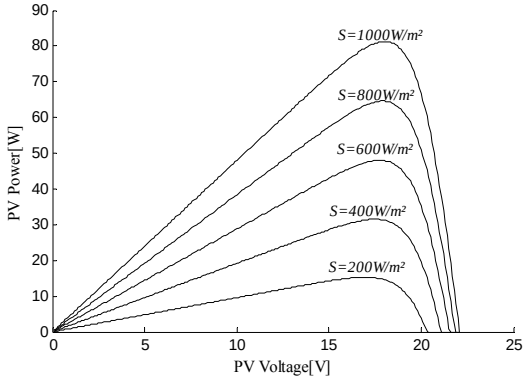

Figure 4. PV P-V characteristic for several irradiation levels.

The current generated by a PV cell is directly dependent on the solar irradiance S. Increasing cell temperature decreases the open circuit voltage, while the short circuit current slightly increases. The cell efficiency thus decreases. The MPPT coordinates are recorded for different irradiation levels in Table I.

TABLE I. THE VOLTAGE AND CURRENT AT MPP FOR IRRADIANCE VARIATION

***S* [W/m^2]**	***Vmpp* [V]**	***Impp* [A]**
200	17	0.8979
400	17.5	1.8013
600	17.7	2.7121
800	17.9	3.6087
1000	18	4.5134

III. DC-DC BOOST CONVERTER

Fig. 5 shows the block diagram of a current-controlled Boost converter. The circuit has two states: when the switch S_T is closed or open.

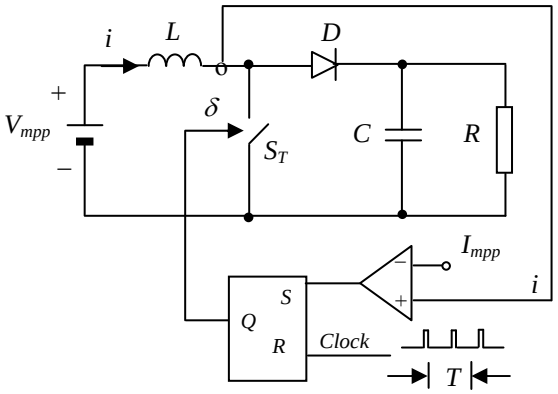

Figure 5. The current-mode controlled Boost converter.

When the switch S_T is closed, the input V_{mpp} provides energy to the inductor L, the current grows linearly and all clock pulses are ignored. The circuit is described by two uncoupled differential state equations described by:

$$\begin{cases} \dfrac{dv}{dt} = -\dfrac{v}{RC} \\ \dfrac{di}{dt} = \dfrac{V_{in}}{L} \end{cases} \tag{2}$$

When the current i reaches the I_{mpp} current the switch S_T is opened: the current i falls; the circuit is now described by a pair of coupled first-order differential equations. The switch S_T is then closed again, on the occurrence of a clock pulse occurs.

$$\begin{cases} \dfrac{dv}{dt} = -\dfrac{v}{RC} + \dfrac{i}{C} \\ \dfrac{di}{dt} = -\dfrac{v}{L} + \dfrac{V_{mpp}}{L} \end{cases} \tag{3}$$

A compact form of the state equations is expressed as

$$\dot{x}(t) = \begin{cases} A_{on} \cdot x + B_{on} \cdot u, & S_T \text{ is on} \\ A_{off} \cdot x + B_{off} \cdot u, & S_T \text{ is off}. \end{cases} \tag{4}$$

where $x = (v\ ;\ i)$ denotes the state vector of the circuit and the matrices A and B are given by:

$$A_{on} = \begin{bmatrix} -\dfrac{1}{RC} & 0 \\ 0 & 0 \end{bmatrix}, \qquad A_{off} = \begin{bmatrix} -\dfrac{1}{RC} & \dfrac{1}{C} \\ -\dfrac{1}{L} & 0 \end{bmatrix} \tag{5}$$

and

$$B_{on} = B_{off} = \begin{bmatrix} 0 \\ \dfrac{1}{L} \end{bmatrix}, \qquad u = V_{mpp}. \tag{6}$$

The following Boost parameters values are used: L = 0.5 mH, C = 75 μF and T = 40 μs. The value of the inductor L and the switching frequency f are chosen so that discontinuous conduction is avoided. The value of the capacitor is chosen so that the output voltage ripple be small.

The Boost converter's inputs are the voltage V_{mpp} and current I_{mpp} produced by the solar panel. I_{mpp} is directly proportional to the solar irradiance S, which represents the first bifurcation parameter. Therefore, the other circuit parameters are kept constant for the observation of the behavior of the Boost converter, while only the solar irradiance S varies.

The current i is observed for a fundamental period – T waveform, then for a period – $2T$ subharmonic waveform and finally to a chaotic waveform, starting from small values of S and progressively increasing its magnitude.

Fig. 6 shows the simulation waveform of the inductor current i for the period – T orbit with S = 200 W/m^2. It illustrates that the period – T trajectory is bounded by i between around 0.5 A and 0.9 A. Fig. 7 shows the phase portrait of i and output voltage v. The power spectrum of the inductance current i is only composed of the fundamental frequency (a sharp peak at 25 kHz) and its harmonics, as shown in Fig. 8.

The period – $2T$ waveform is also periodic. It is called period – $2T$ because the pattern of a large peak followed by a small peak is repeated approximately once even two cycles of the period – T signal. The period – $2T$ waveform is repeated roughly every 0.08 ms; this periodic signal has a fundamental frequency of 1.25 kHz, as shown in Fig. 11. The phase portrait is shown in Fig. 10, with the boundaries of i from around 0.8 A and 1.8 A.

Fig. 12, 13 and 14 present the chaotic case when S = 1000 W/m^2. As shown in Fig. 14, the no periodicity power spectrum of the inductance current $i(t)$ is an indicator of the presence of chaos. The whole frequency range is continuously spanned.

It is essential to study the occurrence of chaos due to the variation of system parameters. When a bifurcation occurs, an abrupt change in the steady-state behavior of the system also occurs. A bifurcation diagram represents all the plots of the steady-state orbit in function of a bifurcation parameter. We vary the irradiance S parameter and plot about 600 consecutive values of the inductance current i at each clock frequency in function of S.

Fig. 15 shows the bifurcation diagram. The load is kept constant at 50 Ω, and the irradiance S, which is the bifurcation parameter, is varied between 100 W/m^2 to 1000 W/m^2, with a 10 W/m² step. The Boost converter shows periodic-doubling cascade from period – 1 to chaos. For small values of S, the system is T - periodic, so just one point is visible: all the 600 points fall at the same position.

The first bifurcation takes place at 385 W/m^2, where the period – T bifurcates to period – $2T$. If the system is period – $2T$, two points are visible: 300 points fall at one position (the current i of the large peak at the clock frequency) and 300 points fall at the second position (the current i of the small peak at the clock frequency). For chaos, the result is a set of dots, none of them falling on the other. A bifurcation diagram clearly shows the change of behavior as a parameter is varied.

The bifurcation diagram using the irradiance S as parameter and for a variation of load R between 10 Ω to 40 Ω is presented Fig. 16.

For different values of S and R, one can easily identify the behaviour of the Boost converter: the system is periodic for small values of the load R and irradiance S, while it is chaotic for large value of R and S.

Figure 17 shows the power spectrum of i, when S varies between 100 W/m^2 to 1000 W/m^2, and then decreases to 100 W/m². This variation is a good representation of the irradiance during a whole day, from dawn to nightfall.

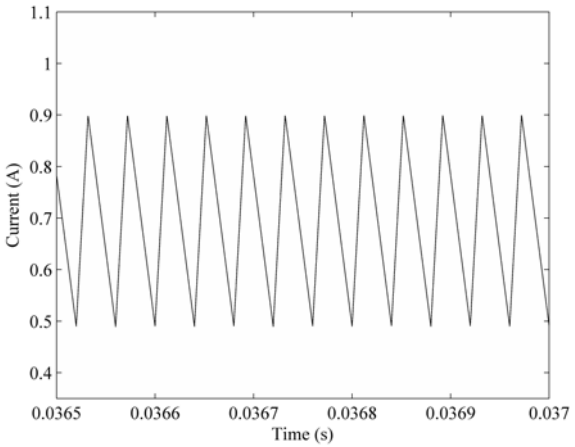

Figure 6. Fundamental current $i(t)$ of the state equation of the Boost converter for S = 200 W/m^2.

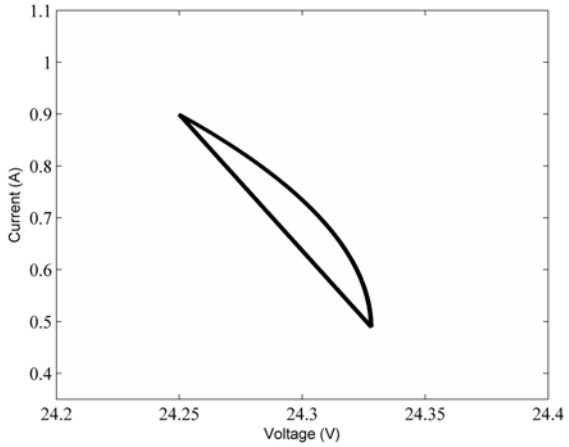

Figure 7. Phase portrait of a fundamental orbit of the state equation of the Boost converter for S = 200 W/m^2.

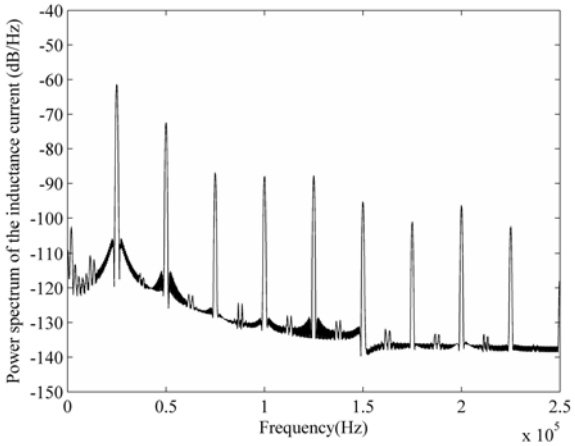

Figure 8. Spectral distribution of inductor current $i(t)$ of the Boost converter for S = 200 W/m^2.

IV. Filippov Method For Boost Converter

It is necessary to calculate the range of the fluctuating variables S and R for which the period – T orbit will remain stable, in order to ensure the stability of the system. Now we proceed to a theoretical identification of the range of S, applying the Filippov method.

The state-space model is

$$\dot{x}(t) = \begin{cases} f_+(x), & S_T \text{ is off} \\ f_-(x), & S_T \text{ is on.} \end{cases} \quad (7)$$

where

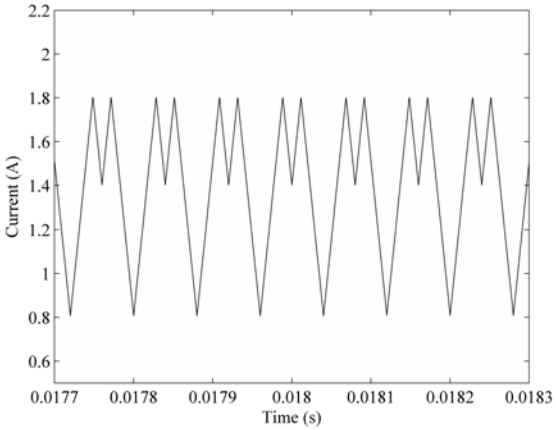

Figure 9. The period - 2*T* subharmonic current *i(t)* of the state equation of the Boost converter for $S = 400$ W/m^2.

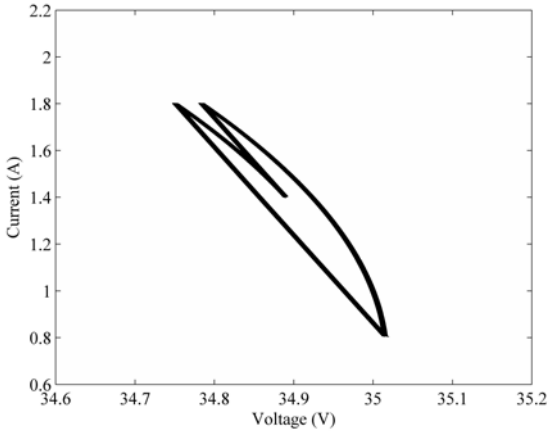

Figure 10. Phase portrait of a period - 2*T* subharmonic orbit of the state equation of the converter for $S = 400$ W/m^2.

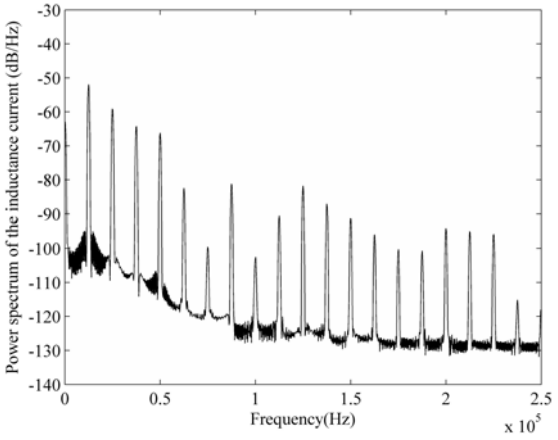

Figure 11. Spectral distribution of inductor current *i(t)* of the Boost converter for $S = 400$ W/m^2.

$$f_+(x) = \begin{bmatrix} \dfrac{Ri - v}{RC} \\ \dfrac{V_{mpp} - v}{L} \end{bmatrix}, \qquad f_-(x) = \begin{bmatrix} \dfrac{-v}{RC} \\ \dfrac{V_{mpp}}{L} \end{bmatrix}. \tag{8}$$

The switching hypersurface *h* [13] is given by

$$h(X(t),t) = i - I_{mpp}. \tag{9}$$

The normal vector *n* determined by the *h* gradient is:

$$n = \nabla h(X,t) = \begin{bmatrix} \dfrac{\partial h}{\partial v} & \dfrac{\partial h}{\partial i} \end{bmatrix}^T = \begin{bmatrix} 0 \\ 1 \end{bmatrix}. \tag{10}$$

For the on period, the state transition matrix is given by $\Phi_-(t,0) = e^{A_{on}t}$ and for the off period, the state transition matrix is $\Phi_+(t, dT) = e^{A_{off}(t - dt)}$,

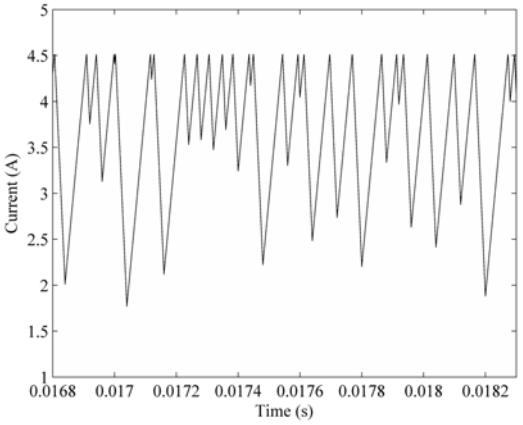

Figure 12. The chaotic inductance current *i(t)* from simulation of the state equation of the Boost converter for $S = 1000$ W/m^2.

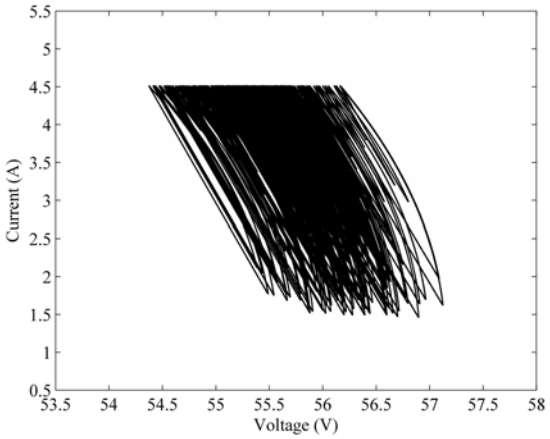

Figure 13. Phase portrait of chaotic orbit from simulation of the state equation of the Boost converter for $S = 1000$ W/m^2.

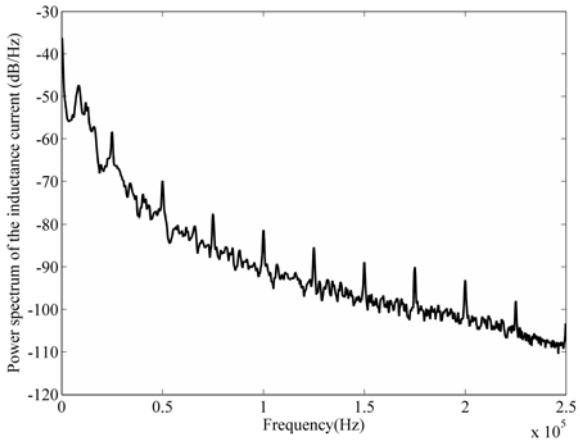

Figure 14. Spectral distribution of inductor current *i(t)* of the Boost converter for $S = 1000$ W/m^2.

where *d* is the duty cycle of the converter.

The saltation matrix [16][17] which describes the transition at the switching event is given by

$$SM = I_2 + \frac{(f_+ - f_-)n^T}{n^T f_- + \dfrac{\partial h}{\partial t}} = \begin{bmatrix} 1 & \dfrac{iL}{V_{mpp}C} \\ 0 & 1 - \dfrac{v}{V_{mpp}} \end{bmatrix}. \tag{11}$$

We are interested in the stability of a periodic - *T* orbit that starts at a specific state *x*(0) at a clock instant, then arrives on the *x(dT)* at the end of the on S_T, and returns to the beginning state at the end of the clock period *x(T)* = *x*(0).

The state transition monodromy matrix over a whole clock cycle (0,*T*) is calculated. Since the switch on is from 0 to

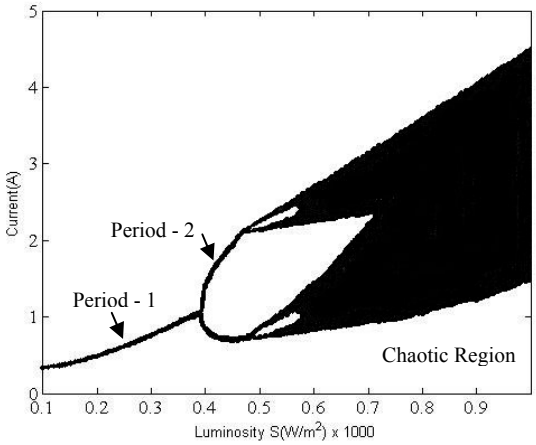

Figure 15. The bifurcation diagram of the inductance current taking *S* as the bifurcation parameter (R = 50 Ω).

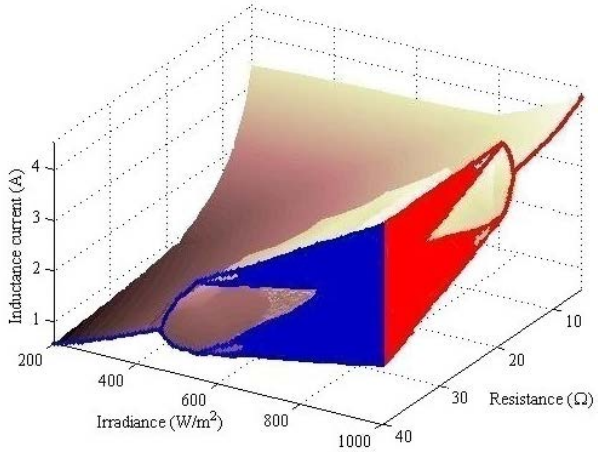

Figure 16. The bifurcation diagrams of the inductance current taking *S* as the bifurcation parameter, and for several values of *R*.

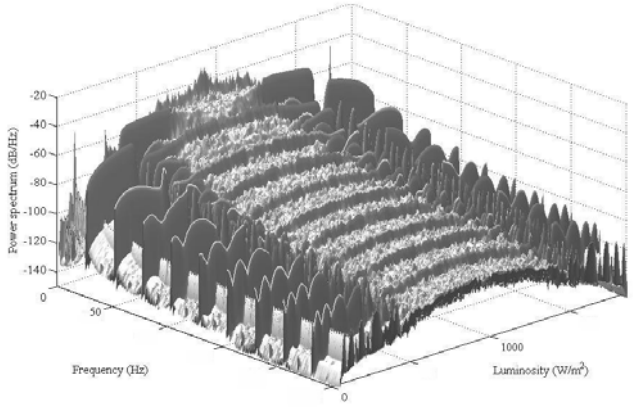

Figure 17. Spectral distribution of inductor current *i(t)* of the Boost converter with irradiance *S* variation.

dT, and the switch off from *dT* to *T*, the monodromy matrix [14] [15] can be described by

$$M = \Phi_{+}(T, dT) \cdot SM \cdot \Phi_{-}(dT, 0). \tag{12}$$

In order to calculate the monodromy matrix and its eigenvalues, the duty cycle *d* needs to be determined. The state vectors at $t = dT$ and $t = T$ can be expressed as:

$$x(dT) = e^{A_{on} dT} \cdot x(0) + \int_0^{dT} e^{A_{on}(dT-\tau)} \cdot \begin{bmatrix} 0 \\ \dfrac{V_{mpp}}{L} \end{bmatrix} d\tau \tag{13}$$

$$x(T) = e^{A_{off}(T-dT)} \cdot x(dT) + \int_{dT}^{T} e^{A_{off}(T-\tau)} \cdot \begin{bmatrix} 0 \\ \dfrac{V_{mpp}}{L} \end{bmatrix} d\tau . \tag{14}$$

Let us remark that $x(T) = x(0)$.

Substituting (13) into (14) and solving for $x(0)$ leads to

$$x(0) = \left(I_2 - e^{A_{off}(T-dT)} \cdot e^{A_{on} dT} \right)^{-1} \cdot \cdot \left[e^{A_{off}(T-dT)} \cdot Int_{on} + Int_{off} \right] \tag{15}$$

where Int_{on} and Int_{off} are the two integrals in (13) and (14). From the hypersurface, we get

$$I_{mpp} = i = \begin{bmatrix} 0 & 1 \end{bmatrix} x(dT). \tag{16}$$

After substituting $x(0)$ from (15) and $x(dT)$ from (13), (16) can be solved numerically with the Newton-Raphson [15] method to obtain the value of d for the periodic orbit.

$$NewtRaphs(d) = \begin{bmatrix} 0 & 1 \end{bmatrix} \left\{ e^{A_{on} dT} \cdot \left(I_2 - e^{A_{off}(T-dT)} \cdot e^{A_{on} dT} \right)^{-1} \cdot \left[e^{A_{off}(T-dT)} \cdot Int_{on} + Int_{off} \right] + Int_{on} \right\} - I_{mpp}. \tag{17}$$

Once these values are found, the monodromy matrix can be expressed as a function of irradiance *S*, and its eigenvalues can be calculated. Fig.18 shows the eigenvalues of the system for different values of the *S*.

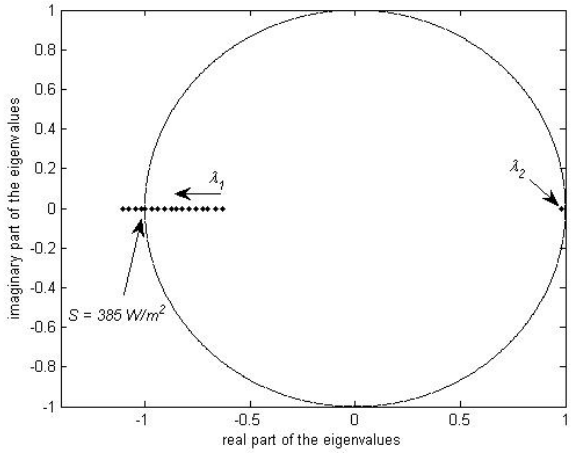

Figure 18. Locus of characteristic multipliers as *S* varies.

For S = 300 W/m^2 and R = 50 Ω, the solution of the Newton-Raphson expression is $d = 0.4273$. We get

$$x(0) = \begin{bmatrix} 30.261 \\ 0.7585 \end{bmatrix} \text{ and } x(dT) = \begin{bmatrix} 29.972 \\ 1.3498 \end{bmatrix} \tag{18}$$

The saltation and monodromy matrices are

$$SM = \begin{bmatrix} 1 & 0.2923 \\ 0 & -0.7492 \end{bmatrix} \qquad M = \begin{bmatrix} 0.9824 & 0.0608 \\ -0.0453 & -0.7573 \end{bmatrix} \tag{19}$$

The eigenvalues of the monodromy matrix are $\lambda_1 = 0.98087$ and $\lambda_2 = -0.75572$.

A bifurcation is described by any crossing from the interior of the unit circle to the exterior. It is the case for the irradiance value of S = 385 W/m^2. We can generate the loci of eigenvalues using (12). The typical loci are exemplified in Table II, which are graphically illustrated in Fig. 18. The loci indicate a period-2*T* as *S* varies. By the Filippov method, one can obtain the range of *S* and *R* for which the eigenvalues are inside the unit circle, leading to a stable periodic-*T* operation (Fig. 19). The design limits are set with this diagram.

Let us take the example of the photovoltaic solar potential in Europe [16], given in Fig. 20. If the photovoltaic system has a large value of *R*, the designer will have to ensure that

the variations of irradiance *S* keep the system within the stable region of the Fig.19. For example, this system used in the South of Europe, i.e. with a large variation of irradiance *S*, will mainly be unstable. It is therefore much better to choose a solar system with a small value of *R* (Fig. 19). It can then be used without any irradiance or geographical restriction.

TABLE II. EIGENVALUES FOR DIFFERENT VALUES OF *S*

***S* [W/m^2]**	**Charat. Mult. λ_1, λ_2**	**Remarks**
200	-0.43557 and 0.9779	Stable 1T
300	-0.75572 and 0.98087	Stable 1T
385	-1.00078 and 0.9815	Period-doubling
400	-1.45787 and 0.98159	Period-doubling
450	-1.17758 and 0.9817	Period-doubling

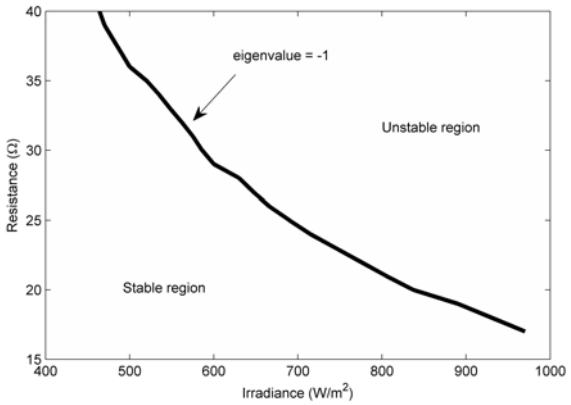

Figure 19. Region of stability of the period – 1 orbit.

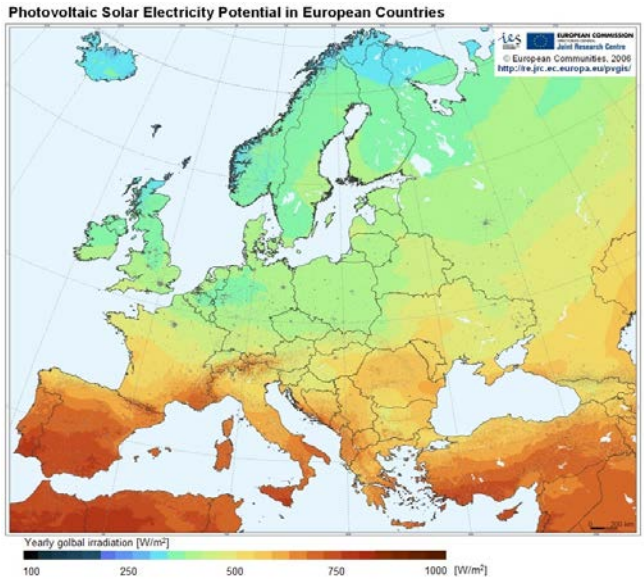

Figure 20. The photovoltaic solar potential in Europe.

V. CONCLUSION

This paper describes bifurcation phenomena of a photovoltaic system. The behaviour of the Boost converter is thoroughly studied: the system is periodic, quasi-periodic or chaotic for different values of irradiance and load. The range of these external parameters is determined for a stable periodic operation, using the Filippov method. This investigation is important to predict nonlinear phenomena and for the components dimensioning for a (steady state mode) proper functioning.

REFERENCES

[1] W. Xiao, N. Ozog, and W. G. Dunford, "Topology Study of Photovoltaic Interface for Maximum Power Point Tracking, " *IEEE Transactions on Industrial Electronics*, vol. 54, no. 3, pp. 1696-1704, 2007.

[2] M. J. Vasallo Vázquez, J. M. Andújar Márquez, and F. S. Manzano, "A Methodology for Optimizing Stand-Alone PV-System Size Using Parallel-Connected DC/DC Converters, " *IEEE Transactions on Industrial Electronics*, vol. 55, no. 7, pp. 2664-2673, 2008.

[3] D. Petreus, D. Moga, A. Rusu, T. Patarau, M. Munteanu, "Photovoltaic System with Smart Tracking of the Optimal Working Point, " *Advances in Electrical and Computer Engineering*, vol. 10, no. 3, pp. 40-47, 2010. Available: http://dx.doi.org/10.4316/ AECE. 2010.03007.

[4] D. Petreus, T. Patarau, S. Dărăban, C. Morel, B. Morley, "A Novel Maximum Power Point Tracker Based on Analog and Digital Control Loops" *Solar Energy*, vol. 85, pp.588-600, 2011.

[5] V. Salas, E. Olias, A. Barrado, and A. Lazaro, "Review of the maximum power point tracking algorithms for stand-alone photovoltaic systems," *Solar Energy Materials and Solar Cells*, vol. 90, pp. 1555-1578, 2006.

[6] A. Pandey, N. Dasgupta and A. K. Mukerjee, "High-Performance Algorithms for Drift Avoidance and Fast Tracking in Solar MPPT System," *IEEE Transactions on Energy Conversion*, vol. 23, no. 2, 2008. Available: 10.1109/TEC.2007.914201

[7] T. Esram, P. L. Chapman, "Comparison of Photovoltaic Array Maximum Power Point Tracking Techniques", *IEEE Transactions on Energy Conversion*, vol. 22, no. 2, pp. 439 – 449, 2007. Available: doi:10.1109/TEC.2006.874230.

[8] Z. Wujian, L. Qiuhua et al, "Survey of Maximum Power Point Tracking Techniques for Photovoltaic Array," *High Voltage Engineering*, Vol.34, No.6, pp.1145-1154, 2008.

[9] C. Morel, R. Vlad, J-Y. Morel, "Anticontrol of Chaos Reduces Spectral Emissions," *Journal of Computational and Nonlinear Dynamics*, vol. 3, pp. 041009-1, 2008.

[10] C. Morel, M. Bourcerie, F. Chapeau-Blondeau, "Generating independent chaotic attractors by chaos anticontrol in nonlinear circuits," *Chaos, Solitons and Fractals*, vol. 26, pp. 541, 2005.

[11] C. Morel, R. Vlad, E. Chauveau, "A new technique to generate independent periodic attractors in the state space of nonlinear dynamic systems," *Nonlinear Dynamics*, vol. 59, pp. 45, 2009.

[12] M. G. Villalva, J. R. Gazoli, E. Ruppert F., Comprehensive approach to modeling and simulation of photovoltaic arrays, *IEEE Transactions on Power Electronics*, vol. 25, no. 5, pp. 1198 – 1208, 2009. Available: 10.1109/TPEL.2009.2013862.

[13] D. Giaouris, S. Banerjee, B. Zahawi, V. Pickert, "Stability analysis of the continuous-conduction-mode Buck converter via Filippov's method," *IEEE Transaction on Circuits and Systems*, vol. 55, no.4, 2008.

[14] D. Giaouris, S. Banerjee, B. Zahawi, V. Pickert, "Control of fast scale bifurcations in power-factor correction converters," *IEEE Transaction on Circuits and Systems*, vol. 54, no.9, 2007.

[15] D. Giaouris, S. Maity, S. Banerjee, B. Zahawi, V. Pickert, "Application of Filippov method for the analysis of subharmonic instability in dc-dc converters," *International Journal of Circuit Theory and Applications*, vol. 37, 2009.

[16] M. Šúri, T.A. Huld, E.D. Dunlop, H.A. Ossenbrink, 2007. Potential of solar electricity generation in the European Union member states and candidate countries. *Solar Energy*, 81, 1295–1305, http://re.jrc.ec.europa.eu/pvgis/countries/europe.htm.